Case Studies in Thermal Engineering 73 (2025) 106545

Contents lists available at ScienceDirect

Case Studies in Thermal Engineering

journal homepage: www.elsevier.com/locate/csite

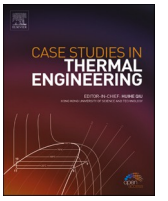

# The thermal conductivity characteristics and prediction models of limestone sand-yellow soil mixtures

Xiong Liu [a], Ruiyong Mao [a,*], Zujing Zhang [a], Hongwei Wu [b], Xing Liang [c], Jing Chen [d]

[a] College of Civil Engineering, Guizhou Provincial Key Laboratory of Rock and Soil Mechanics and Engineering Safety, Guizhou University, Guiyang, 550025, China
[b] School of Physics, Engineering and Computer Science, University of Hertfordshire, Hatfield, AL10 9AB, UK
[c] School of Computer Science and Mathematics, Kingston University London, KT1 2EE, UK
[d] Guizhou Polytechnic of Construction, Guiyang, 550025, China

ARTICLE INFO

*Keywords:*
Ground source heat pump
Backfill material
Gradation
Sand-soil mixture
BP neural network prediction

ABSTRACT

To optimize the backfilling of ground source heat pump drilling mud and boost the thermal conductivity of drilling materials, this study proposes using a mixture of limestone sand and loess, typical in karst regions, as backfill for buried pipe heat exchangers. Through indoor experiments, 152 limestone sand-loess mixtures were prepared and their thermal conductivities tested. Analyses explored the impacts of limestone sand content, moisture content, dry density, and particle size distribution. Results show that artificially graded materials generally outperform natural ones in thermal conductivity, with grading's influence decreasing as moisture rises. At 8 % moisture, grading increases thermal conductivity by 18.57 % (0.069–0.124 W/(m·K)); at 20 %, the increase is 7.63 %. High moisture and limestone sand content can yield a thermal conductivity of 1.508 W/(m·K). When using graded materials, geological conditions and aquifers should be considered, and they suit strata with moderate moisture. A backpropagation neural network - based predictive model for thermal conductivity, developed from experimental data, achieved 6.4 % average absolute percentage error, indicating good accuracy.

## 1. Introduction

As a renewable energy source, geothermal energy offers significant advantages, including substantial reserves, widespread distribution, and environmental cleanliness [1–3]. It holds considerable potential for development. Meanwhile, the ground source heat pump (GSHP) represents an energy-efficient system that harnesses shallow geothermal energy for heating and cooling buildings. This system has garnered considerable attention due to its benefits, such as stable year-round operation, high heat exchange efficiency, and contributions to energy conservation and environmental protection [4,5]. The GSHP system facilitates heat exchange with the surrounding geotechnical medium through an underground heat exchanger. The backfill material functions as the heat exchange medium between the underground heat exchanger and the surrounding geotechnical body, and its thermal conductivity is essential for enhancing the overall heat exchange performance of the GSHP [6].

Enhancing the thermal conductivity of backfill materials is crucial for boosting the heat exchange capacity and improving the heat

* Corresponding author.
*E-mail address:* rymao@gzu.edu.cn (R. Mao).

https://doi.org/10.1016/j.csite.2025.106545
Received 7 May 2025; Received in revised form 16 June 2025; Accepted 19 June 2025
Available online 20 June 2025

transfer efficiency of heat exchangers. To this end, a diverse range of backfill materials has been developed. These include sand - bentonite - based composites [7], cement - based mixtures [8], phase change materials [9,10], quartz sand as a bentonite substitute [11], and high - thermal - conductivity additives such as graphite [12] and steel slag [13,14]. Previous studies have demonstrated that an appropriate increase in the thermal conductivity of backfill materials can effectively augment the heat exchange of heat exchangers, reduce the total borehole length [15,16], and mitigate thermal buildup [17]. With the continuous advancement and widespread adoption of ground source heat pump systems, the development of high - thermal - conductivity materials and novel phase change materials has emerged as a focal point in the research on backfill materials. However, modern new materials encounter significant challenges. Their development is often arduous and costly, resulting in elevated initial investment expenses. Moreover, much of the research on these advanced materials remains confined to numerical simulations, with limited practical application in real - world projects. In general, traditional backfill materials (including pure and mixed materials) are still predominantly used in ground source heat pump systems, accounting for approximately 90 % of applications, compared to only 10 % for modern backfill materials [18]. Consequently, there is an urgent need to explore the reprocessing of drilling grouts, which holds great promise for enhancing the operational efficiency of buried - pipe systems.

Although high thermal conductivity is generally beneficial for heat exchangers, for backfill materials in ground - source heat pump systems, higher values do not always guarantee improved performance. Research suggests that the optimal thermal conductivity of backfill materials should be marginally higher than that of the surrounding rock and soil [19]. Drilling mud, with its thermal conductivity closely matching that of the original soil layer, is considered a suitable candidate for backfilling. However, direct use of untreated drilling mud can undermine the efficiency of ground - source heat pump systems. This inefficiency can occur due to stratification within the backfilled layers, causing a mismatch in thermal conductivity between the drilling mud and the underlying strata, or because of inconsistent particle sizes in the mud, which can negatively impact the compactness of the backfill [20]. These issues can lead to a decrease in thermal conductivity, ultimately deteriorating the heat exchange performance between the heat exchanger and the surrounding rock. As a result, reprocessing the main aggregates of drilling mud to enhance its thermal conductivity for backfilling represents a more effective approach. In karst regions, where the geology of ground - source heat pump drilling is predominantly bedrock, using highly conductive bedrock gravel as backfill material is advisable. For example, previous studies have shown that adding silica sand to bentonite slurry can increase the thermal conductivity of the enhanced bentonite slurry by 30 % [21]. Compared with the development of high - thermal - conductivity materials and phase - change materials, backfilling with the original slurry is more cost - effective and environmentally friendly. Drilling mud is mainly composed of sand, gravel, and soil, and sandy soil is a three - phase mixture of solid, liquid, and gas [22]. Its thermal conductivity is affected by factors such as aggregate content [23], particle size [24], moisture content, and dry density [25]. Given the complex heat - transfer mechanism involved, further investigation is required. Thus, it is essential to explore the effects and underlying mechanisms of factors like aggregate content, moisture content, and particle size on thermal conductivity.

The sand-soil mixtures obtained from drilling slurry exhibit low thermal conductivity. To enhance the thermal conductivity of these mixtures, one can utilize sand and gravel with superior thermal conductivity, increase the aggregate content, and modify the particle sizes to expand the contact area between particles. For instance, Kong et al. [26] addressed the low thermal conductivity of loess in the Loess Plateau region by incorporating iron tailings, which possess better thermal conductivity, as an aggregate. Similarly, Xu et al. [27] proposed a waste steel slag-calcium clay mixture as a backfill material for buried pipelines. In addition to selecting materials with improved thermal conductivity as aggregates, both researchers also employed grading techniques to enhance the void space between particles, thereby increasing the contact area and, consequently, improving the thermal conductivity of the backfill material. Grading significantly influences heat and mass transfer among particles in sand-soil mixtures. Wen et al. [28] examined the pore structure characteristics and hydraulic properties of granite residual soils with varying particle grading. Nagaraj et al. [29] experimentally assessed the impact of the sand proportion and its grading on the undrained strength behavior of the soil, while Liu et al. [30] manipulated particle size and grading to modify the number and volume of pores, thereby affecting the calcium carbonate precipitation process. Particle grading can enhance the mutual contact area among soil particles and influence the proportional distribution of solids, water, and air, which directly impacts the thermal conductivity of the mixture [31,32]. Therefore, incorporating particle grading into sand-soil mixtures and reusing limestone sand as a thermally conductive aggregate presents a cost-effective and efficient method for improving the thermal conductivity of drilling slurries.

Numerous factors influence the thermal conductivity of soil, rendering the relationship between soil thermal conductivity and its influencing factors quite intricate [33–35]. While traditional theories and experimental models of soil thermal conductivity have addressed the labor-intensive nature of experimental measurements, most models are applicable only to specific soil types or conditions, which do not accurately represent real-world scenarios, resulting in certain distortions in predictive outcomes [36,37]. With the advancement of machine learning techniques, neural network algorithms have gained widespread application in predicting the properties of various materials [38–40], including the thermal conductivity of materials based on dry density and moisture content [41]. These algorithms can establish more precise models that correlate thermal conductivity with numerous influencing factors [42, 43], thus becoming a powerful tool for addressing complex thermal conductivity function formulas [44–47]. Consequently, employing neural network algorithms to develop a thermal conductivity prediction model for limestone sand-loess mixtures presents a viable approach to enhancing the accuracy of predictive data.

In conclusion, previous researchers and scholars have conducted comprehensive studies on the thermal conductivity of soil and sand. Most investigations concerning backfill materials have primarily focused on cement grouting, bentonite-based materials, and the development of novel phase-change backfill materials. However, there is a relative scarcity of studies on the utilization of sand-soil mixtures for backfill purposes [48]. Researchers have frequently concentrated on pure materials rather than mixed materials when examining traditional backfill options for buried pipe heat exchangers. Furthermore, the mechanisms governing the coupled heat

transfer relationship between the thermal conductivity of the mixture and influencing factors such as moisture content, dry density, and gradation remain unclear, necessitating additional sample data for further research and clarification. This paper selects common loess from the surface and limestone-based sand and gravel from the karst region as aggregates for investigation and analysis. The dry density, water content, and thermal conductivity of sand-soil mixtures were measured, and the impact of material properties on thermal conductivity was examined using scanning electron microscopy (SEM). Additionally, the varying degrees of influence that changes in gradation have on the thermal conductivity of materials under different water contents of sand-soil mixtures were comparatively analyzed. A nonlinear BP neural network prediction model for the thermal conductivity of limestone-soil mixed materials was developed and optimized. It is also recommended that to enhance the heat transfer efficiency of GSHP systems, appropriate material gradation should be selected based on the specific engineering geology and underground aquifer conditions.

## 2. Experimental research

### 2.1. Experimental materials

The aggregate materials used in this experiment were sourced from the drilling slurry of a local GSHP project. The primary component of the slurry was limestone, and loess was selected from the common loess found at the project site. The basic physical properties of these materials are provided in Tables 1 and 2. The physical parameters of the materials were measured in accordance with Wan et al. [49]. Specific gravity, density, and moisture content were determined using the specific gravity meter method and the ring knife method. The weight difference before and after oven drying was used to calculate moisture content. Additionally, the void ratio and dry density were calculated based on the measured density, moisture content, and specific gravity.

The liquid and plastic limits were determined using the combined liquid-plastic limit method, with the plasticity index being calculated as the difference between the liquid limit and the plastic limit. Limestone, a primary component of karst terrain, is mainly composed of calcite and possesses excellent properties, including high thermal conductivity, strength, water absorption, impermeability, sound insulation, polish, cementation, and workability.

### 2.2. Description of experimental apparatus

The FOX50 thermal conduction meter is a testing instrument for the heat transfer coefficient that complies with ASTM and ISO 8301 standards. It features a temperature measurement range from −10 to 110 °C and a thermal conductivity measurement range from 0.1 to 10 W/(m·K). The measurement accuracy is ±3 %. The optical encoder facilitates the most precise digital measurement of sample thickness. Its unique thin film thermal flow sensor provides a distinctive measurement of thermal flux density. Sample dimensions are in the form of circular disks with a diameter of 50 mm and a height varying between 10 and 20 mm. Upon launching the instrument's software, set the temperatures for the top and bottom cold and hot plates, and then insert the test sample into the gap between the two plates, which will automatically close after the test. The operational procedure for the thermal conductivity tester is illustrated in Fig. 1.

The FOX50 thermal conductivity tester primarily comprises a thermal conductivity main unit, a circulating water cooler, and a nitrogen bottle. The thermal conductivity main unit is designed to hold the test materials, while the water cooler supplies the upper and lower plate temperatures necessary for the operation of the thermal conductivity tester. Additionally, the nitrogen bottle provides the force required to press the upper and lower plates of the thermal conductivity tester together. The tablet press is capable of compressing the materials into a disc shape, thereby facilitating the measurement of the thermal conductivity coefficient of the materials. The instrument is illustrated in Fig. 2.

### 2.3. Sequential experimental procedures

Crush the limestone gravel and loess into granular form using a crusher, and then bake in an oven at 120 °C for 24 h until dry. The materials are categorized into natural gradation and artificial gradation. The experimental materials consist of crushed rock mass and soil, which must be analyzed using sieve analysis to establish the natural gradation curve. Select characteristic ranges that encompass coarse, medium, and fine particles, with the sample's natural gradation concentrated within the range of 0.1–20 mm. At this stage, four ranges can be identified: 0∼1.5 mm (very fine), 0.5∼2 mm (fine), 2∼5 mm (medium), 5∼10 mm (coarse), and 10∼20 mm (gravel), ensuring the inclusion of key parameters such as the 10 % passing particle size, 60 % median particle size, and 90 % passing particle size [50,51]. For the natural gradation component, simply mix the materials according to the specified proportions. For the artificial gradation component, the materials are screened using international standard sieves with particle sizes of 0.16 mm, 0.25 mm, 0.315 mm, 0.63 mm, 1 mm, 1.25 mm, 2.5 mm, 3 mm, 5 mm, and 8 mm, and then mixed according to the specified proportions to create artificial gradation materials.

**Table 1**
Basic physical properties of loess material.

| Parameter | Dry density (g/cm$^3$) | Density (g/cm$^3$) | Moisture content (%) | Specific gravity | Void ratio | Plastic limit (%) | Liquid limit (%) | Plasticity index (%) |
|---|---|---|---|---|---|---|---|---|
| Value | 1.52 | 1.68 | 12.3 | 3.42 | 0.75 | 19.36 | 13.53 | 32.89 |

**Table 2**
Basic physical properties of limestone sand material.

| Parameter | Specific gravity | Dry density (g/cm$^3$) | Moisture content (%) | Void ratio |
|---|---|---|---|---|
| Value | 2.66 | 1.68 | 22.6 | 0.7 |

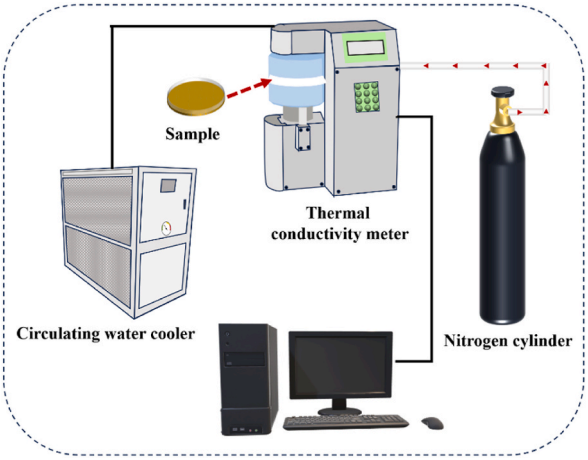


**Fig. 1.** Schematic diagram of the FOX50 heat flow meter method for thermal conductivity testing.

(a) Conductometer (b) Water cooler (c) Nitrogen cylinder (d) Tablet press

**Fig. 2.** Experimental equipment.

Thus, the materials were categorized into two groups: natural grading and manmade grading. The five test materials (loess, mixture 1, mixture 2, mixture 3, and limestone) were denoted as (L, LM1, LM2 and LM3, S), where the natural graded limestone gravel was referred to as NS, and mixture 3 in the manmade grading category was abbreviated as MM3. The grading and proportions of the test materials used in this study are listed in Table 3. The grading curves were determined using the sieve analysis method, and the corresponding grading curves of the test materials are presented in the figure below. These curves reflect the particle size distribution of the soil, enabling the determination of the percentage of the total dry weight represented by each particle size range.

In geotechnical engineering, the grading coefficient ($C_c$) and the uniformity coefficient ($C_u$) are used to assess the quality of soil gradation. The corresponding calculation methods are outlined below:

**Table 3**
Mixing ratios and quantities of materials.

| Material composition | Gradation | |
|---|---|---|
| | Natural gradation | Manmade gradation |
| Loess ((100 % Loess+0 % Limestone) | NC | MC |
| Mixture 1 ((70 % Loess+30 % Limestone) | NM1 | MM1 |
| Mixture 2 ((50 % Loess+50 % Limestone) | NM2 | MM2 |
| Mixture 3 ((30 % Loess+70 % Limestone) | NM3 | MM3 |
| Limestone (0 % Loess+100 % Limestone) | NS | MS |

$$C_c = \frac{d_{30}^2}{d_{10} \times d_{60}} \tag{1}$$

$$C_c = \frac{d_{60}}{d_{10}} \tag{2}$$

where $d_{10}$,$d_{30}$,$d_{60}$ represent specific particle sizes (in mm), corresponding to the diameters on the particle size distribution curve where 10 %, 30 %, and 60 % of the total mass of particles are smaller than these values, respectively. A larger value of the uniformity coefficient $C_u$ indicates a more dispersed particle composition, while the grading coefficient $C_c$ reflects whether the particle size distribution curve lacks an intermediate range of soil particles. According to standard textbooks and national specifications, a soil gradation is considered good if the grading coefficient $C_c$ lies between 1 and 3, and the uniformity coefficient $C_u$ is greater than 5. Otherwise, the gradation is deemed poor. In this study, the natural graded limestone exhibited a uniformity coefficient $C_u = 10$ and a grading coefficient $C_c = 19.36$. For the natural loess gradation, $C_u = 5.5$ and $C_c = 0.88$. The manmade limestone gradation had $C_u = 13.3$ and $C_c = 2.1$, while the manmade loess gradation showed $C_u = 6.6$ and $C_c = 2.2$. Based on these results, it can be concluded that the natural gradations of loess and limestone do not meet the criteria for optimal gradation, whereas the manmade gradations satisfy the required standards. The corresponding gradation curves are shown in Fig. 3 below.

Mix the dry limestone sand and loess in varying proportions uniformly, then add an appropriate amount of water, stir, and fill the molds. Utilize a small hydraulic pump to compact the mixture, applying pressure to achieve a set pressure of 30 MPa for 30 s to facilitate setting. Subsequently, place the molds in an oven at 120 °C for 48 h to dry, with the objective of allowing the loess and limestone sand mixture to dry and set. After stabilizing the shape, measure the height to determine the volume of a single sample, and weigh its dry weight using a balance. Calculate the dry density value based on the mass-to-volume ratio. Determine the amount of water required based on the dry weight and moisture content, and uniformly drip pure water into the sample using a dropper. Seal the sample and allow it to sit for 24 h to ensure even distribution of moisture, then measure its thermal conductivity. The quantity of water added each time is calculated based on the target moisture content, and the aforementioned steps are repeated for each moisture content to create four samples.

In order to investigate the effect of moisture content on the thermal conductivity of backfill materials, water was added to dry-formed loess and limestone sand, as well as their mixtures, at specified mass percentages. The experimental materials consist of porous media such as soil and rock, with natural moisture content typically ranging from 0 % to 30 %. According to the data presented in Tables 1 and 2, the initial moisture content of the limestone and loess utilized in this study is 22.6 % and 12.3 %, respectively. Furthermore, the moisture content range of the materials must encompass typical working conditions including dry state, moderate humidity, and near saturation. A specific gradient pattern is maintained throughout the moisture content tests, with the moisture content of the materials controlled at 2 %, 8 %, 14 %, and 20 %, thereby covering common humidity levels encountered in most engineering scenarios (the moisture content of soil layers above the groundwater level is generally <15 %), which corresponds to the sensitive variation range of material mechanical properties [52,53]. The moisture content of limestone sand cannot be measured for thermal conductivity when it reaches 20 %; therefore, its moisture content is controlled at 2 %, 8 %, and 14 %. The experimental scheme for measuring the thermal conductivity of the mixed backfill is outlined in Table 4.

### 2.4. Validation of experimental reliability

The thermal conductivity meter must adhere to specific accuracy standards when measuring thermal conductivity. However, due to potential setup errors or measurement inaccuracies, the thermal conductivity values obtained from the instrument may not be reliable. Therefore, it is essential to verify the errors associated with the thermal conductivity meter. Under room temperature conditions, the upper and lower plates are maintained at temperatures of 30 °C and 10 °C, respectively. The ordinary crown glass sample is measured four times under these specified temperature conditions, with the results being calibrated against the established standard thermal conductivity. It is recognized that the standard thermal conductivity of ordinary crown glass at the aforementioned temperature

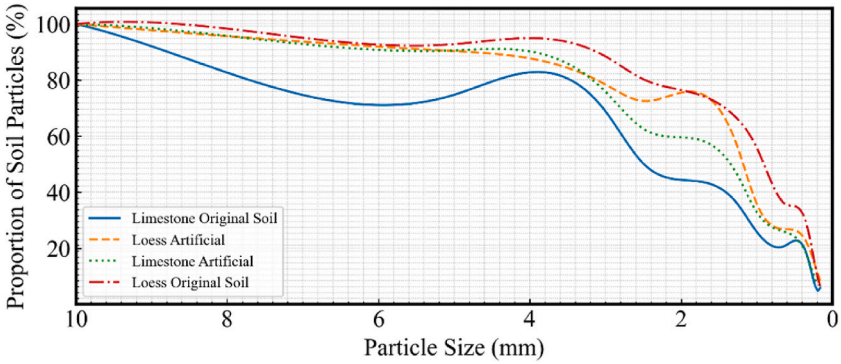


**Fig. 3.** Material gradation curve.

**Table 4**
Experimental protocol for measuring thermal conductivity of materials.

| Group | Material type | ω/% | ρ/(g/cm$^3$) | | | |
|---|---|---|---|---|---|---|
| | | | NO.1 | NO.2 | NO.3 | NO.4 |
| 1 | NC | 2 % | 1.684 | 1.719 | 1.783 | 1.827 |
| 2 | NC | 8 % | 1.323 | 1.424 | 1.506 | 1.543 |
| 3 | NC | 14 % | 1.603 | 1.704 | 1.758 | 1.833 |
| 4 | NC | 20 % | 1.463 | 1.546 | 1.618 | 1.677 |
| 5 | MC | 2 % | 1.716 | 1.784 | 1.826 | 1.864 |
| 6 | MC | 8 % | 1.374 | 1.474 | 1.558 | 1.612 |
| 7 | MC | 14 % | 1.618 | 1.727 | 1.783 | 1.853 |
| 8 | MC | 20 % | 1.483 | 1.608 | 1.659 | 1.737 |
| 9 | NS | 2 % | 1.726 | 1.862 | 1.974 | 2.015 |
| 10 | NS | 8 % | 1.822 | 1.858 | 1.945 | 2.054 |
| 11 | NS | 14 % | 1.829 | 1.903 | 1.984 | 2.032 |
| 12 | MS | 2 % | 1.753 | 1.854 | 1.945 | 2.054 |
| 13 | MS | 8 % | 1.845 | 1.922 | 1.984 | 2.074 |
| 14 | MS | 14 % | 1.856 | 1.905 | 1.953 | 2.054 |
| 15 | NM1 | 2 % | 1.524 | 1.663 | 1.712 | 1.788 |
| 16 | NM1 | 8 % | 1.631 | 1.785 | 1.832 | 1.865 |
| 17 | NM1 | 14 % | 1.733 | 1.826 | 1.913 | 1.957 |
| 18 | NM1 | 20 % | 1.467 | 1.586 | 1.628 | 1.682 |
| 19 | MM1 | 2 % | 1.579 | 1.655 | 1.748 | 1.834 |
| 20 | MM1 | 8 % | 1.683 | 1.748 | 1.837 | 1.922 |
| 21 | MM1 | 14 % | 1.783 | 1.854 | 1.963 | 2.043 |
| 22 | MM1 | 20 % | 1.532 | 1.583 | 1.673 | 1.743 |
| 23 | NM2 | 2 % | 1.688 | 1.732 | 1.843 | 1.955 |
| 24 | NM2 | 8 % | 1.583 | 1.633 | 1.764 | 1.829 |
| 25 | NM2 | 14 % | 1.727 | 1.834 | 1.894 | 2.044 |
| 26 | NM2 | 20 % | 1.622 | 1.762 | 1.864 | 1.918 |
| 27 | MM2 | 2 % | 1.753 | 1.783 | 1.837 | 1.894 |
| 28 | MM2 | 8 % | 1.628 | 1.684 | 1.753 | 1.846 |
| 29 | MM2 | 14 % | 1.755 | 1.832 | 1.926 | 2.063 |
| 30 | MM2 | 20 % | 1.654 | 1.734 | 1.828 | 1.934 |
| 31 | NM3 | 2 % | 1.583 | 1.653 | 1.732 | 1.867 |
| 32 | NM3 | 8 % | 1.639 | 1.724 | 1.844 | 1.919 |
| 33 | NM3 | 14 % | 1.694 | 1.763 | 1.832 | 1.915 |
| 34 | NM3 | 20 % | 1.832 | 1.921 | 2.062 | 2.127 |
| 35 | MM3 | 2 % | 1.635 | 1.743 | 1.864 | 1.974 |
| 36 | MM3 | 8 % | 1.688 | 1.787 | 1.863 | 1.978 |
| 37 | MM3 | 14 % | 1.715 | 1.783 | 1.873 | 1.933 |
| 38 | MM3 | 20 % | 1.843 | 1.963 | 2.073 | 2.183 |

settings is 1.0 W/(m·K). As presented in Table 5, the relative error for each measurement group remains below 1 %, indicating that the thermal conductivity testing instrument satisfies the required accuracy for operational use.

Due to various reasons, the experimental materials cause a certain deviation in measuring the true values, so it is necessary to introduce uncertainty in assessing the measurement quality of the experimental results [54]. According to the technical parameters found in the manual of the FOX50 thermal conductivity tester, its testing accuracy is ±3 %, and reproducibility is ±2 %.

Accuracy serves as a component of system uncertainty, representing the deviation of measurement results from the true value. It is typically regarded as expanded uncertainty, utilizing a factor of k = 2, which indicates that it encompasses approximately 95.4 % of the measurement values. Consequently, the standard uncertainty is calculated as $u_1 = 3\,\%/2 = 1.5\,\%$. Reproducibility, on the other hand, constitutes a component of random uncertainty, reflecting the extent of dispersion observed in multiple measurements. Likewise, it is also treated as expanded uncertainty, resulting in a standard uncertainty of $u_2 = 2\,\%/2 = 1\,\%$. The combined standard uncertainty, $u_c$, can be derived as follows:

$$u_c = \sqrt{u_1 + u_2} = \sqrt{1.5^2 + 1^2} = 1.80\% \tag{3}$$

This level of accuracy complies with the standards set for scientific research (1.8 % < 2 %), and the reliability of the result is

**Table 5**
Calibration results of the thermal conductivity meter.

| Test Number | Thermal conductivity (W/(m·K)) | Residual (W/(m·K)) | Relative error (%) |
|---|---|---|---|
| 1 | 0.9984 | −0.0016 | −0.16 |
| 2 | 0.9985 | −0.0015 | −0.15 |
| 3 | 1.0021 | 0.0021 | 0.21 |
| 4 | 0.9982 | −0.0018 | −0.18 |

significantly high.

## 3. Results and discussion

### 3.1. Effect of material properties on thermal conductivity

The thermal conductivity of backfill materials is influenced by the properties and structural characteristics of the constituent materials. Fig. 4 presents the SEM images of loess and limestone sand. As shown in Fig. 4 (a), at a magnification of 500×, the loess particles appear as powdery clumps with numerous surface cracks. At a higher magnification of 5000× (Fig. 4 (b)), the surface structure of loess reveals a small amount of flocculent texture. In contrast, Fig. 4 (c) and 4 (d) illustrate that limestone sand particles exhibit varying block sizes, with numerous voids between the particles and a lack of stable structural cohesion. The surface of the limestone sand is characterized by numerous razor-like features.

Limestone sand particles have high hardness but exhibit uneven particle sizes and poor bonding, while loess particles are smaller, uniform, and possess good cohesion, which contributes to its lower thermal conductivity. Although limestone sand has a higher intrinsic thermal conductivity, the numerous internal voids within the mixture result in insufficient particle contact, and the trapped air within these voids increases the thermal resistance of the material. This limits the heat transfer efficiency in the borehole. In contrast, the fine, cohesive nature of loess compensates for the drawbacks of limestone sand, such as its large voids and lack of compactness. Therefore, mixing limestone sand with loess is expected to enhance the overall thermal conductivity of the composite material compared to the individual components.

To evaluate the impact of material properties on thermal conductivity, the variation in thermal conductivity with respect to dry density was analyzed for materials containing 70 % limestone sand and gravel, as well as 100 % limestone sand and gravel, at moisture contents of 2 % and 14 %. As shown in Fig. 5, the thermal conductivity of all materials increases with an increase in dry density. Additionally, the thermal conductivity of the manmade gradation materials generally exceeds that of the naturally graded materials. In Fig. 5 (a), it can be observed that the thermal conductivity of NS (natural graded limestone sand) is higher than that of NM3 (man-made graded material 3), and the thermal conductivity of NM3 is higher than that of NC (natural graded loess), indicating that an increase in limestone sand content enhances the thermal conductivity of the material. Furthermore, the effect of grading on the thermal conductivity varies with different limestone sand contents, suggesting that both the material composition and grading significantly influence the thermal conductivity performance.

As the moisture content increases from 2 % to 14 %, it is observed that the difference in thermal conductivity between NS (natural graded limestone sand) and NM3 (man-made graded material 3) decreases. In contrast, the change in thermal conductivity between NC (natural graded loess) and NM3 is not significant. This phenomenon can be attributed to the increased contact area between the loess

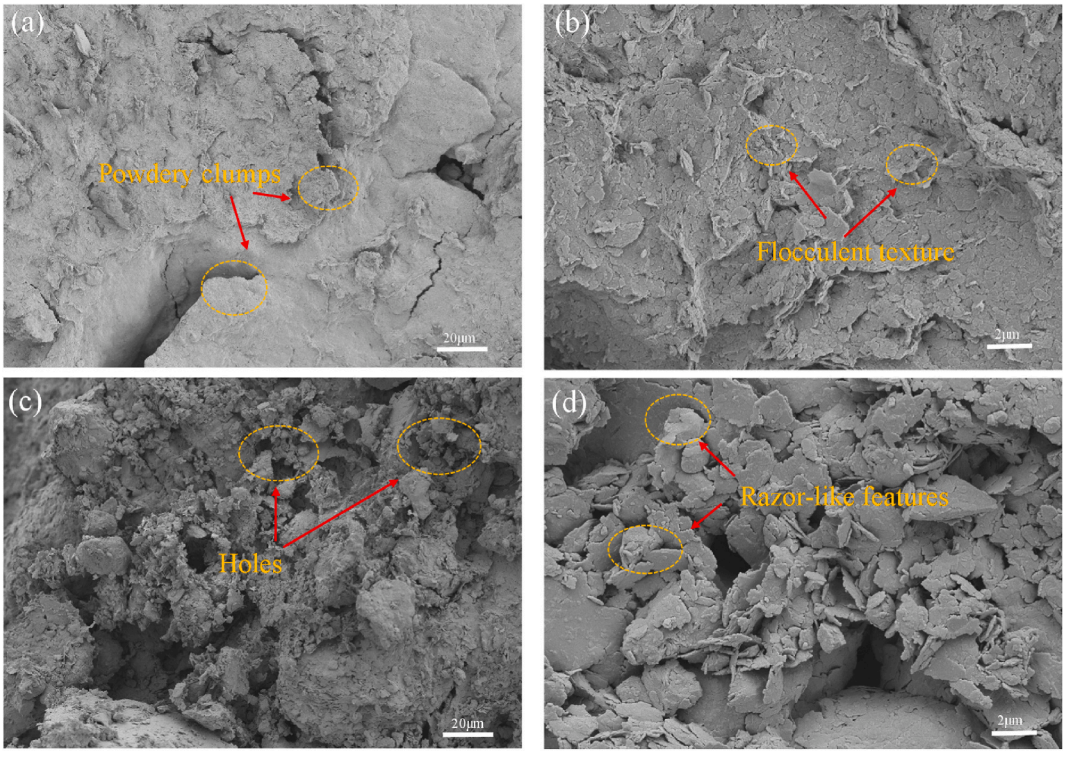


**Fig. 4.** SEM images of loess and limestone sand: (a) Loess ( × 500); (b) Loess ( × 5000); (c) Limestone sand ( × 500); (d) Limestone sand ( × 5000).

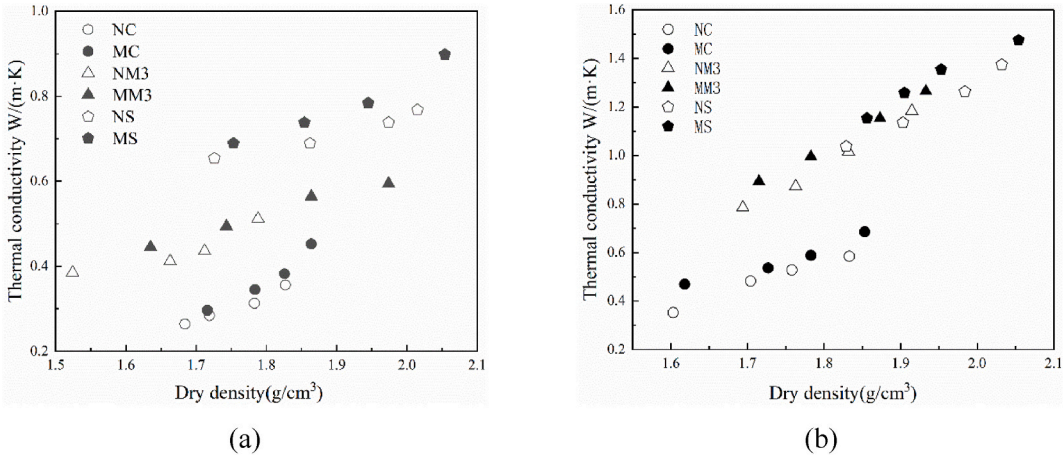


**Fig. 5.** Thermal conductivity of differently graded materials at 2 % and 14 % moisture content. (a) ω = 2 %; (b) ω = 14 %.

and limestone sand particles after mixing, with moisture filling the interstitial spaces and forming liquid bridges. This coupling effect enhances heat transfer between the materials. Additionally, the overall thermal conductivity of the manmade gradation material is superior to that of the naturally graded material. This improvement is due to the gradation process, which fills the voids between particles, reduces the particle size gaps, and increases material density. The enhanced density, combined with the effect of moisture, further improves the heat transfer performance. The thermal conductivity of the materials under varying moisture content is shown in Fig. 6.

### 3.2. *Effect of dry density and moisture content on thermal conductivity*

The sand-soil mixture, as a solid-liquid-gas three-phase mixture, is significantly influenced by both moisture content and dry density in terms of thermal conductivity. The dry density of the material is governed by factors such as porosity, void size, particle size distribution, void curvature, and structural characteristics. Dry density plays a crucial role in determining the thermal conductivity of a porous medium. As moisture fills the voids between particles, it displaces the air, and since water has a higher thermal conductivity than air, the presence of moisture substantially enhances the overall thermal conductivity of the material. To assess the influence of dry density and moisture content on thermal conductivity, the maximum moisture content of the materials was set to 20 %, with limestone sand having a maximum moisture content of 14 % and the minimum moisture content of all materials set at 2 %. The variation in thermal conductivity with respect to dry density at the minimum and maximum moisture contents for each material is illustrated in Fig. 7.

It is illustrated in Fig. 7 that the thermal conductivity of both man-made graded and natural graded materials increases with rising dry density and moisture content. The impact of dry density and moisture content on thermal conductivity is more pronounced at higher moisture levels. For instance, when the dry density of natural loess increased from 1.684 g/cm$^3$ to 1.827 g/cm$^3$ at a moisture content of 2 %, the thermal conductivity increased from 0.284 W/(m·K) to 0.356 W/(m·K), representing a 25.35 % increase. At a moisture content of 20 %, the dry density of natural loess increased from 1.463 g/cm$^3$ to 1.677 g/cm$^3$, and the thermal conductivity increased from 0.683 W/(m·K) to 0.853 W/(m·K), a 24.89 % increase.

For manmade loess, at 2 % moisture content, the dry density increased from 1.716 g/cm$^3$ to 1.864 g/cm$^3$, and the thermal

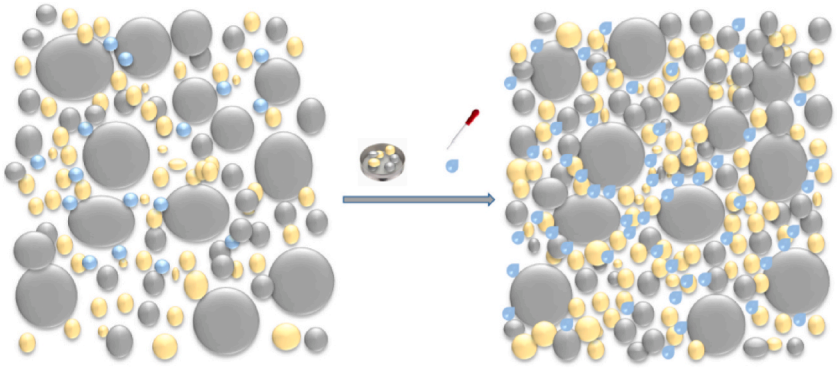

**Fig. 6.** Schematic illustration of the effect of grade change and moisture to improve heat transfer materials.

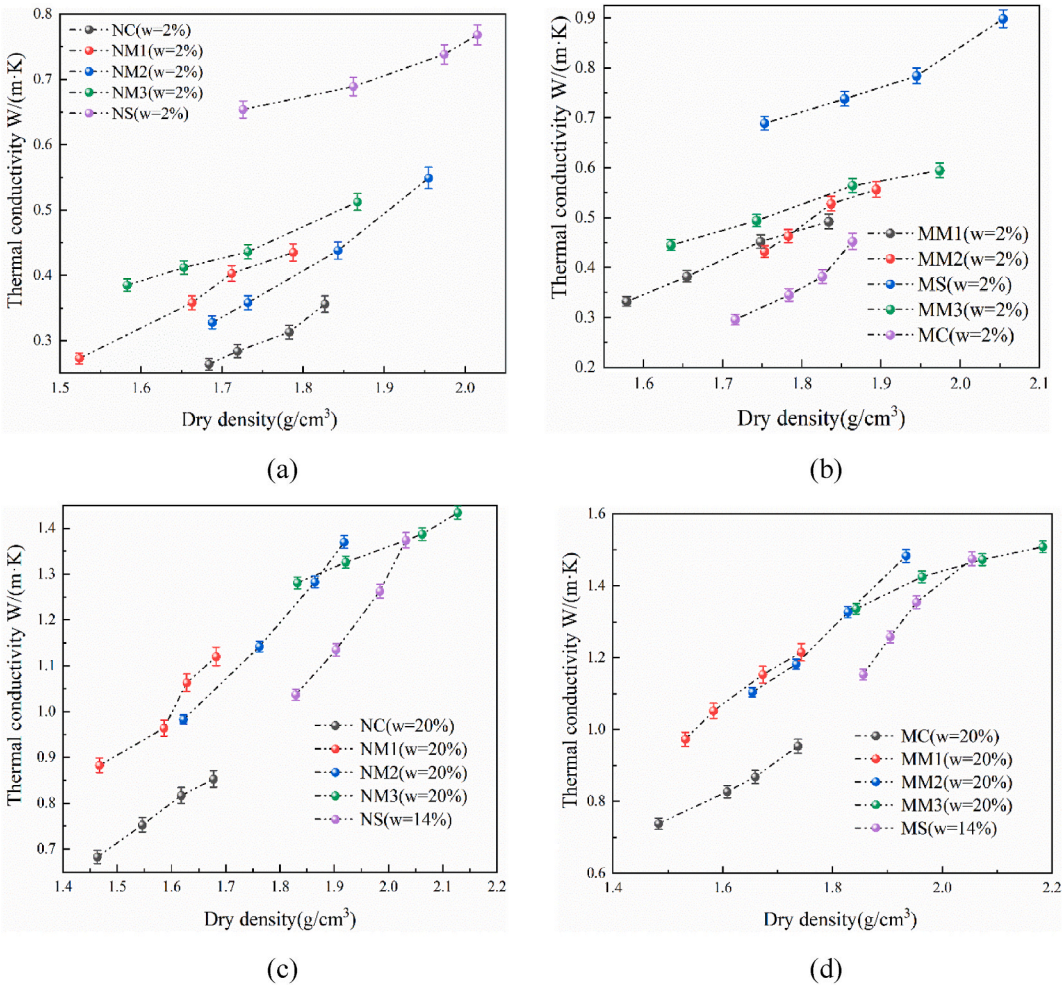


**Fig. 7.** Relationship between thermal conductivity and dry density for different materials at the same moisture content: (a) Natural graded material (ω = 2 %); (b) Manmade gradation sample material (ω = 2 %); (c) Natural graded material (ω = 14 %); (d) Manmade gradation material (ω = 14 %).

conductivity rose from 0.296 W/(m·K) to 0.452 W/(m·K). At 20 % moisture content, the dry density of manmade loess increased from 1.483 g/cm$^3$ to 1.737 g/cm$^3$, with thermal conductivity increasing from 0.738 W/(m·K) to 0.954 W/(m·K), corresponding to increases of 52.70 % and 29.26 %, respectively.

In general, samples with higher moisture content and dry density exhibit higher thermal conductivity. The effect of moisture content on thermal conductivity is more significant than that of dry density. At lower moisture content, the thermal conductivity of each material increases moderately with rising dry density. However, at higher moisture content, the increase in thermal conductivity becomes more rapid.

### *3.3. Effect of gradation on thermal conductivity of materials under different moisture content conditions*

Effective gradation enhances the compaction of sand-soil mixtures, which is directly reflected in the dry density of the material. Manmade gradation sample materials typically exhibit slightly higher or more favorable thermal conductivity compared to naturally graded materials. However, the thermal conductivity of graded materials varies under different moisture contents and limestone sand contents. To assess and analyze the influence of gradation on thermal conductivity, error bars representing the standard deviation are presented for materials with different moisture contents.

#### *3.3.1. The effect of gradation on the thermal conductivity of materials at 2 % moisture content*

The dry density histograms and thermal conductivity curves for both man-made and naturally graded materials at a moisture content of 2 % are presented in Fig. 8. It is evident from the figure that both the thermal conductivity and dry density of man-made graded materials are generally superior to those of natural graded materials.

As shown in Fig. 8, an increase in limestone sand content leads to a corresponding increase in the thermal conductivity of both man-

made and natural graded materials, with a gradual upward trend. This is attributed to the enhanced thermal conductivity resulting from the higher limestone sand content, with the most significant increase observed when the limestone sand content rises from 70 % to 100 %.

The most direct effect on thermal conductivity at low moisture content is the increase in the proportion of aggregate. However, when both limestone sand content and moisture content are fixed, manmade gradation can further enhance the material's thermal conductivity. As shown in Table 6, at 2 % moisture content, for a given limestone sand content, grading leads to an increase in thermal conductivity ranging from 9.12 % to 21.23 %, corresponding to a change in thermal conductivity of 0.055–0.088 W/(m·K).

Among the materials, loess shows the greatest improvement in thermal conductivity after grading, followed by Mix 3. As the limestone content increases, the rate of thermal conductivity improvement due to grading in loess is 21.33 %, with a tendency to stabilize in the middle range. The lowest improvement of 9.12 % is observed when the limestone sand content reaches 100 %.

### *3.3.2. The effect of gradation on the thermal conductivity of materials at 8 % moisture content*

Fig. 9 illustrates the thermal conductivity of artificial graded materials and natural graded materials at a moisture content of 8 %. At this moisture level, as the content of limestone sand increases, the thermal conductivity of both natural and artificial graded materials displays a similar increasing trend. Furthermore, the thermal conductivity of artificial graded materials consistently surpasses that of natural materials, with the most rapid growth rate observed when the limestone sand content constitutes 50 %–70 %, demonstrating a pattern of initially gradual and subsequently steep increase.

Compared to the growth rate of thermal conductivity at 2 % moisture content, the fastest increase occurs in the range of 50 %–70 % limestone sand content at 8 % moisture content. This can be attributed to the significant impact of moisture amount and distribution on the thermal conductivity of the soil. In dry or low-moisture soils, heat transfer primarily relies on contact point conduction. As moisture content increases, capillary action forms liquid bridges between solid soil particles, enhancing particle contact points and thereby improving thermal conductivity. Since water has a higher thermal conductivity than air, the replacement of air in the soil's voids with water further strengthens heat transfer, making increased moisture content a contributing factor to improved thermal conductivity.

As shown in Table 7, the increase in thermal conductivity due to gradation ranges from 13.81 % to 33.77 % at 8 % moisture content, with changes in thermal conductivity ranging from 0.069 to 0.124 W/(m·K). The increase in water content enhanced the improvement in graded loess from 21.23 % at 2 % moisture content to 33.77 % at 8 % moisture content. This can be attributed to the fact that well-graded materials improve particle structure, and with higher water content, water can more effectively fill the voids to form liquid bridges, which further enhances heat transfer. Additionally, with an increase in limestone sand content, the trend in the increase of thermal conductivity for graded materials remains consistent with that observed at 2 % moisture content.

### *3.3.3. The effect of gradation on the thermal conductivity of materials at 14 % moisture content*

The thermal conductivity of natural and man-made graded materials at 14 % moisture content is presented in Fig. 10. At this moisture level, as the proportion of limestone sand increases, the thermal conductivity improves at a faster rate than at the lower moisture contents. Notably, the gap between the thermal conductivity coefficients of natural and man-made grades diminishes, suggesting that as water content increases, the influence of gradation on the thermal conductivity coefficient weakens. Furthermore, with higher moisture content, the rate of change in thermal conductivity for materials with limestone sand content from 0 % to 50 % is faster than the rate observed at 2 % and 8 % moisture content, indicating a more pronounced effect of moisture on heat transfer in this range.

As shown in Table 8, at a moisture content of 14 %, the increase in thermal conductivity due to gradation ranges from 8.96 % to 17.05 %, with the change in thermal conductivity spanning from 0.083 to 0.113 W/(m·K). As the limestone sand content increases, the influence of gradation on the rate of thermal conductivity increase gradually diminishes.

With rising water content, the enhancement of thermal conductivity in graded material pairs becomes more influenced by the reduction in moisture content. Compared to 8 % moisture content, at 14 %, the thermal conductivity of materials with limestone sand content ranging from 0 % to 50 % shows a faster change trend, and the overall impact on thermal conductivity is more pronounced. At

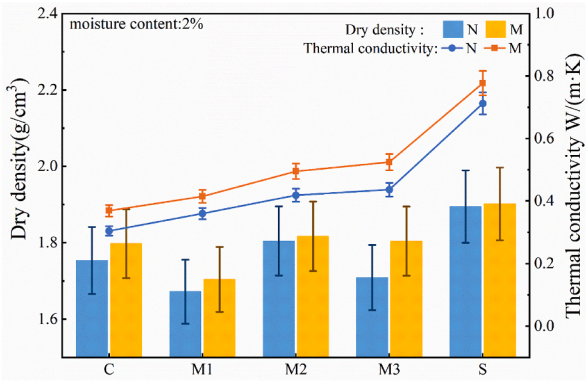


**Fig. 8.** Thermal conductivity of natural and man-made graded materials at 2 % moisture content.

**Table 6**
Increase in thermal conductivity of materials due to gradation at 2 % moisture content.

| Materials | Dry density (g/cm$^3$) | | Thermal conductivity change (W/(m·K)) | Growth rate (%) |
|---|---|---|---|---|
| | Natural gradation | Manmade gradation | | |
| Loess | 1.753 | 1.798 | 0.065 | 21.23 % |
| Mixture 1 | 1.672 | 1.704 | 0.055 | 15.22 % |
| Mixture 2 | 1.804 | 1.817 | 0.077 | 18.32 % |
| Mixture 3 | 1.709 | 1.804 | 0.088 | 20.17 % |
| Limestone | 1.894 | 1.902 | 0.065 | 9.12 % |

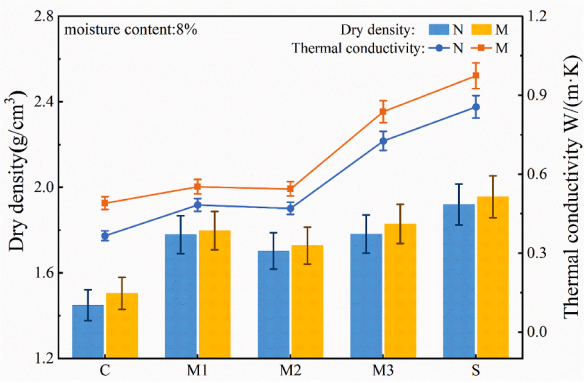


**Fig. 9.** Thermal conductivity of natural and manmade gradation materials at 8 % moisture content.

**Table 7**
Increase in thermal conductivity due to gradation of materials at 8 % moisture content.

| Materials | Dry density (g/cm$^3$) | | Thermal conductivity change (W/(m·K)) | Growth rate (%) |
|---|---|---|---|---|
| | Natural gradation | Manmade gradation | | |
| Loess | 1.449 | 1.505 | 0.124 | 33.77 % |
| Mixture 1 | 1.778 | 1.798 | 0.069 | 14.29 % |
| Mixture 2 | 1.702 | 1.728 | 0.074 | 15.66 % |
| Mixture 3 | 1.782 | 1.829 | 0.111 | 15.31 % |
| Limestone | 1.920 | 1.956 | 0.118 | 13.81 % |

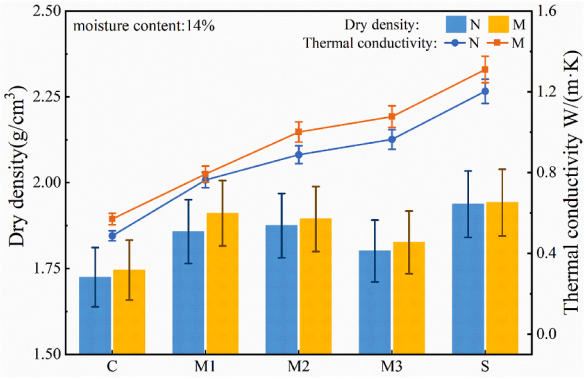


**Fig. 10.** Thermal conductivity of natural and manmade gradation materials at 14 % moisture content.

this stage, the distribution of moisture increases, not only surrounding the particle contact points but also filling the voids within the soil, with most of the air being replaced by water. This results in water connecting the pores in the soil. Therefore, as moisture content increases, the impact of water on thermal conductivity becomes more significant, while the influence of gradation on thermal conductivity diminishes.

**Table 8**
Increase in thermal conductivity of materials due to gradation at 14 % moisture content.

| Materials | Dry density (g/cm$^3$) | | Thermal conductivity change (W/(m·K)) | Growth rate (%) |
|---|---|---|---|---|
| | Natural gradation | Manmade gradation | | |
| Loess | 1.725 | 1.745 | 0.083 | 17.05 % |
| Mixture 1 | 1.857 | 1.911 | 0.099 | 14.31 % |
| Mixture 2 | 1.875 | 1.894 | 0.112 | 12.67 % |
| Mixture 3 | 1.801 | 1.826 | 0.113 | 11.70 % |
| Limestone | 1.937 | 1.942 | 0.108 | 8.96 % |

### *3.3.4. The effect of gradation on the thermal conductivity of materials at 20 % moisture content*

As shown in Fig. 11, at a moisture content of 20 %, the thermal conductivity of both natural and man-made graded materials increases linearly with the increase in limestone sand content, ranging from 0 % to 100 %. At this high moisture content, the sand-soil mixture is saturated with moisture, and the impact of gradation on the thermal conductivity becomes negligible. In this case, the limestone sand aggregate content predominantly influences the thermal conductivity. It is evident that as the moisture content increases from 2 % to 20 %, the effect of gradation on the material's thermal conductivity progressively diminishes.

From Table 9, it is evident that at a moisture content of 20 %, the increase in thermal conductivity resulting from grading ranges from 5.79 % to 9.04 %, corresponding to a change in thermal conductivity of 0.070–0.091 W/(m·K). At this moisture level, the effect of grading on thermal conductivity is minimal, with the increase in thermal conductivity at a moisture content of 20 % being 2.38 to 3.73 times greater than the increase caused by grading at a moisture content of 8 %. Furthermore, as the proportion of limestone sand increases, the impact of grading on the rate of increase in the material's thermal conductivity exhibits a progressively decreasing trend, with the increase in thermal conductivity for mixture 3 due to grading being merely 5.79 %.

Under the various moisture content conditions outlined above, the thermal conductivity of artificial materials consistently surpasses that of natural materials due to the influence of grading. Table 10 presents the composition of bentonite-based backfill materials along with their thermal conductivity [55]. In artificial graded materials, at a moisture content of 20 %, the thermal conductivity of MM2 is measured at 1.483 W/(m·K), which is comparable to that of conventional bentonite-based backfill materials containing 20 % bentonite and 80 % quartz sand. However, traditional bentonite-based backfill materials, Sodium-based bentonite, for example, is priced at CNY 800–1500/t. Resulting in higher investment costs for ground source heat pumps. Moreover, bentonite exhibits expansion upon contact with water and contraction when it loses moisture, potentially leading to voids and disrupting the continuity of heat transfer. In contrast, limestone sand and loess, when graded, feature closely connected particles that do not expand upon contact with water. Additionally, due to loess's excellent water retention properties, its mixed materials are particularly well-suited for karst regions where groundwater is plentiful.

## 4. BP neural network prediction

### *4.1. Establishment of the BP neural network model*

The construction and fundamental operational principles of neural networks are based on the organization and functional mechanisms of the human brain, serving as a simplified imitation of the complex neural networks found within the brain. The Backpropagation (BP) neural network is the most widely used model in neural network applications.

Its core operational principle is as follows: For $n$ input learning samples "$x_1\ x_2\ x_3\ x_4\ x_5 \ldots\ x_n$ ", the corresponding $m$ output samples "$p_1, p_2, p_3 \ldots p_m$ " are known. The error between the actual output ($z_1\ z_2\ z_3\ z_4\ z_5 \ldots\ z_m$)of the neural network and the target vector ($p_1, p_2, p_3 \ldots p_m$) is used to adjust the weights, such that the predicted output $z$ becomes as close as possible to the desired output $t$, thereby

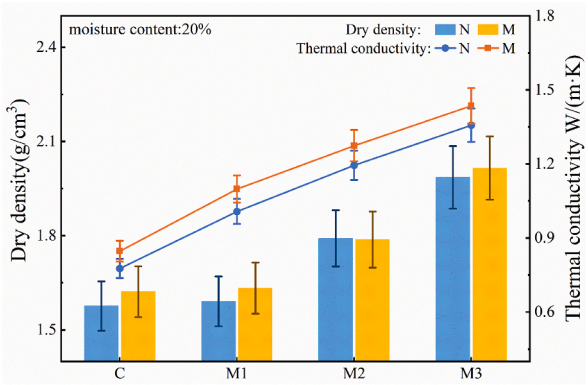


**Fig. 11.** Thermal conductivity of natural and manmade gradation materials at 20 % moisture content.

**Table 9**
Increase in thermal conductivity due to gradation at 20 % moisture content.

| Materials | Dry density (g/cm$^3$) | | Thermal conductivity change (W/(m·K)) | Growth rate (%) |
|---|---|---|---|---|
| | Natural gradation | Manmade gradation | | |
| Loess | 1.576 | 1.622 | 0.070 | 9.04 % |
| Mixture 1 | 1.591 | 1.633 | 0.091 | 9.01 % |
| Mixture 2 | 1.792 | 1.788 | 0.080 | 6.66 % |
| Mixture 3 | 1.986 | 2.016 | 0.079 | 5.79 % |

**Table 10**
Bentonite-based backfill material.

| Bentonite base | Bentonite content | Thermal conductivity (W/(m·K)) |
|---|---|---|
| Backfilling bentonite 1 | Containing 20 %–30 % solids | 0.73–0.75 |
| Backfilling bentonite 2 | Containing 20 % bentonite and 80 % quartz sand | 1.47–1.64 |
| Backfilling bentonite 3 | Containing 15 % bentonite and 85 % quartz sand | 1.00–1.10 |

minimizing the error in the output layer of the network. Through iterative weight adjustments, a BP neural network model is obtained that operates within an acceptable error range.

Assuming that the input vector of the neural network is denoted as X=($x_1$ $x_2$ $x_3$ $x_4$ $x_5$ … $x_n$) T, and the number of neurons in the hidden layer is $h$, the output vector of the hidden layer is then Y= ($y_1$, $y_2$, $y_3$ … $y_h$) T. The number of neurons in the output layer is $m$, and the corresponding output vector of the output layer is Z= ($z_1$, $z_2$, $z_3$, $z_4$, $z_5$ … $z_m$) T. The activation function from the hidden layer to the input layer is denoted as $f$, and the activation function of the output layer is represented by $g$.

Thus there is the output value of the $j$th neuron of the hidden layer:

$$y_j = f\left(\sum_{i=1}^{n} W_{ij}\, x_i - \theta\right) = f\left(\sum_{i=1}^{n} W_{ij}\, x_i\right) \tag{4}$$

The output value of the $k$th neuron of the output layer:

$$z_k = g\left(\sum_{j=0}^{h} w_{jk} y_j\right) \tag{5}$$

The error between the output value and the target value is:

$$\varepsilon = \frac{1}{2}\sum_{k=1}^{m} (t_k - z_k)^2 \tag{6}$$

The weight adjustment formula is:

$$\Delta w_{pq} = -\eta \frac{\delta \varepsilon}{\delta w_{pq}} \tag{7}$$

The normalization function employed in this study is the *Mapmaxmin* function. The syntax for the *Mapmaxmin* function is as follows:

$$y = \frac{(y_{max} - y_{min}) \times (x - x_{min})}{x_{max} - x_{min}} + y_{min} \tag{8}$$

Let $W_{ij}$ denote the synaptic connectivity weights linking the input neuron $i$ in the first layer to the corresponding encrypted neuron $j$ in the subsequent layer. The output value of the input neuron is represented as $x_i$, while $\eta$ denotes the learning rate. The term $\partial\delta\varepsilon/\delta w_{pq}$ represents the partial derivative of the loss function $\varepsilon$ with respect to the weight $w_{pq}$. Additionally, $y$ is the normalized result matrix obtained by standardizing the data matrix $x$.

Subsequently, the *Newff* function is utilized to invoke MATLAB's neural network toolbox, where appropriate parameters are configured: the activation function is set to "*Tansig*", the training algorithm is defined as "*Trainlm*", and the weight update rule is specified by the learning function "*Learngdx*".

*Tansig* hyperbolic tangent *S-shaped* function:

$$f(x) = \frac{2}{1 + e^{-x}} - 1 (-1 < f(x) < 1) \tag{9}$$

The *traingdx* gradient row change rule is:

$$w_{new} = w_{old} - \eta . \nabla E(w_{old}) + \mu . \left(w_{old} - w_{previous}\right) \tag{10}$$

$$b_{new} = b_{old} - \eta.\nabla E(b_{old}) + \mu.\left(b_{old} - b_{previous}\right) \tag{11}$$

The structural design of this model primarily involves determining the number of nodes in the input layer, hidden layer, and output layer, as well as selecting appropriate activation functions. In this study, the factors influencing the thermal conductivity of the limestone sand and loess mixed backfill material are primarily moisture content, dry density, and material type. As illustrated in Fig. 12, given that there are three influencing factors identified in this paper, the number of nodes in the input layer is set at three. The hidden layer is denoted as the Hidden Layer, and following the empirical formula $n_h = \sqrt{n_i + n_o} + a$ (where $n_h$ represents the number of nodes in the hidden layer, $n_i = 3$ is the number of nodes in the input layer, $n_o$ is the number of nodes in the output layer, and a can take values from 1 to 10), after preliminary estimation and experimental adjustments, the number of hidden nodes has been determined to be five.

In this model, both the hidden layer and the output layer utilize the Sigmoid function as the activation function. The various influencing factors demonstrate a complex nonlinear relationship with thermal conductivity, and the Sigmoid function can effectively capture these relationships, thereby enhancing the model's predictive accuracy. The derivative of the Sigmoid function has a straightforward form, facilitating its computation during the error backpropagation process, which is advantageous for the training and optimization of the model. The expression of the Sigmoid function is presented in Eq. (12):

$$\sigma(z) = \frac{1}{1 + e^{-z}} \tag{12}$$

in the equation, $z$ represents the input to the function and may take the form of a scalar, vector, or matrix. When $z$ is a vector, the function will compute each individual element within that vector.

### 4.2. Training and optimization of the BP neural network

After building the prediction model, it is necessary to train the constructed model so that it can meet the actual prediction needs and ensure that the results predicted by this model have considerable reliability. The training parameters for the constructed prediction model are as follows: the number of iterations is set to 1000, the target error is $1 \times 10^{-6}$, and the learning rate is 0.01.

This article performs a Pearson correlation analysis to examine the relationship between various factors and the thermal conductivity test results. The types of materials represent different gradation combinations of limestone and loess. The results of the correlation analysis indicate that the material type, moisture content, and dry density are all positively correlated with the thermal conductivity of the backfill materials, with correlation coefficients of 0.1218 ($P < 0.01$), 0.7544 ($P < 0.01$), and 0.4984 ($P < 0.01$), respectively.

Upon configuring all parameters, the constructed neural network prediction model can be trained using MATLAB. This experiment gathered a total of 152 sets of data. Each experimental dataset includes three influencing factors: material type, moisture content, and dry density, with the output being the thermal conductivity. From this dataset, 130 sets of data were randomly selected to serve as the training set. By inputting this data into the neural network and calculating the error between the network output and the actual values, this paper employs the backpropagation algorithm to iteratively adjust the weights and thresholds of the neural network in order to minimize the prediction error. This process continues through multiple iterations until the error reaches a predetermined threshold or the maximum number of iterations is achieved. Fig. 13 illustrates the error variation curve throughout the network training process. At the 192nd training step, the output error was recorded at 0.00926, thereby satisfying the error target requirement.

Upon completion of the training phase, the remaining 22 datasets were utilized as a test set to evaluate the model's fit and prediction performance. The test set data were input into the trained neural network, which generated the corresponding predicted values. The error between the predicted and actual values was then calculated. The results of both model training and testing are presented in Figs. 14 and 15, where the red line represents the actual values, while the blue line indicates the predicted values generated by the model based on the sample data. The model's fitting performance is depicted in Figs. 16 and 17.

The performance of the model in both training and testing phases was evaluated using several metrics, including the coefficient of determination ($R^2$), mean absolute error (MAE), mean absolute percentage error (MAPE), and root mean square error (RMSE).

The results indicate that the $R^2$ value for the training set is as high as 0.9944, which is very close to 1, suggesting an excellent fit of the model to the training data and that it explains 99.44 % of the variance in the data. This high $R^2$ value demonstrates that the model successfully captures the majority of patterns and information in the training dataset. For the test set, the $R^2$ value is 0.9859, which

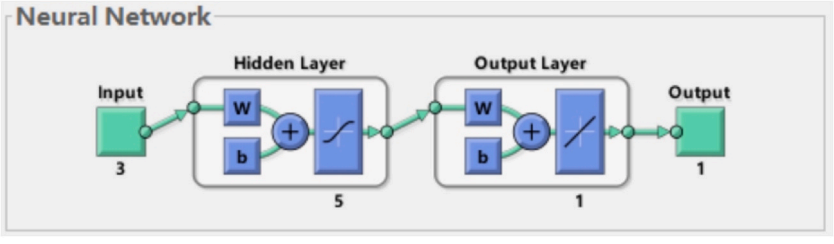


**Fig. 12.** Structure diagram of neural network model.

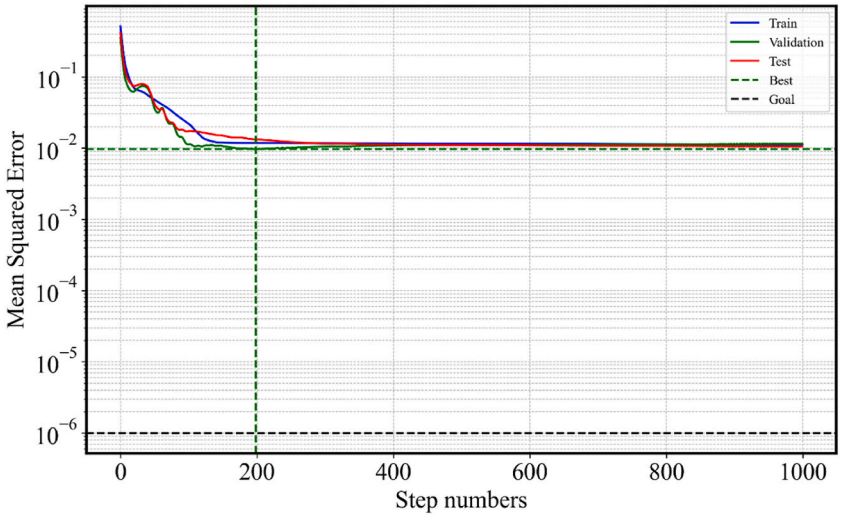


**Fig. 13.** Neural network error variation curve.

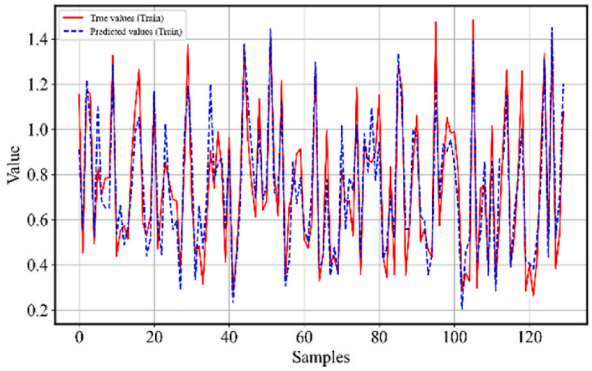


**Fig. 14.** Neural network training results.

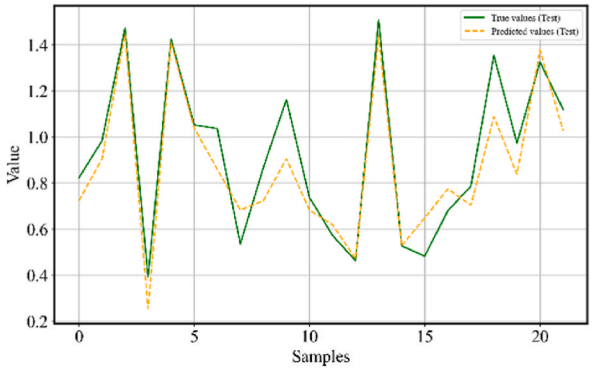


**Fig. 15.** Neural network test results.

remains relatively high, indicating strong generalization ability of the model when applied to new, unseen data. The $R^2$ value exceeding 0.9 for the test set further emphasizes the stability and predictive accuracy of the model.

In addition, the MAE and MAPE values for both the training and test sets reflect the model's solid performance. The MAE for the training set is 0.03, while for the test set, it is even lower at 0.05. The MAPE values for the training and test sets are 4.8 % and 6.4 %, respectively, which are both very low, indicating that the model's prediction accuracy is high.

The RMSE, another critical evaluation metric, also demonstrates the model's predictive capability. The RMSE for the training set is

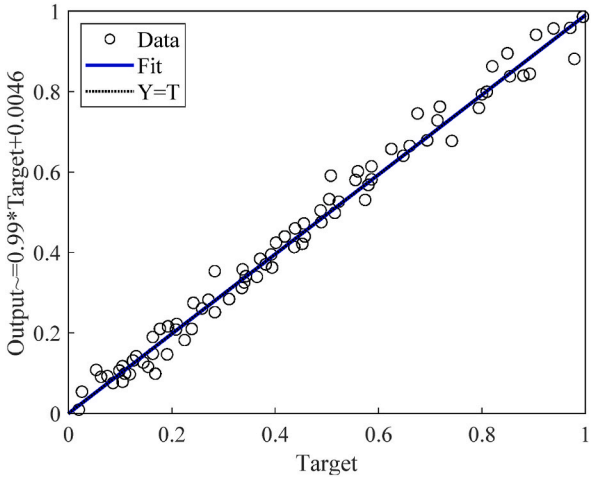


**Fig. 16.** Training set R coefficients.

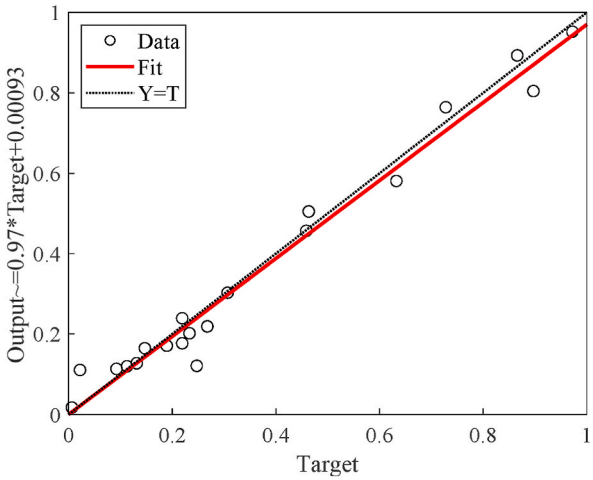


**Fig. 17.** Test set R coefficients.

0.04, and for the test set, it is 0.06. Notably, the RMSE for the test set is lower than that for the training set, suggesting that the model's predicted values are very close to the actual values.

Overall, the BP neural network model effectively predicts the thermal conductivity of materials under various conditions and influencing factors, making it a valuable tool for guiding the design of thermal conductivity in backfill materials for ground-source heat pump systems.

## 5. Conclusion

The thermal conductivity of GSHP backfill materials, specifically sand-soil mixtures, is influenced by various factors. Directly mixing the backfill material may result in issues such as low density and poor thermal conductivity. This study investigates the impact of limestone sand content, moisture content, dry density, and grading on the thermal conductivity of backfill materials composed of limestone sand and loess. The following conclusions are drawn:

(1) Compared to single-component backfills using pure loess or limestone sand alone, the limestone sand-loess mixture constitutes the optimal backfill solution. At a limestone sand content of 70 %, the thermal conductivity of the mixture ranges from 0.358 to 1.483 W/(m·K). When selecting sandy soil mixtures for backfill applications, selective placement strategies can be implemented based on subsurface groundwater levels within the stratum. Experimental results indicate that the limestone sand-loess composite is suitable for selective backfilling under moderate groundwater conditions in the stratum.

(2) As the moisture content and limestone sand content increase, the thermal conductivity of the material exhibits a progressive upward trend. When compared with dry density, the effect of moisture content on thermal conductivity is more significant. In

general, the thermal conductivity of well-graded limestone sand-loess mixtures is higher than that of poorly graded counterparts, with the influence of gradation on mixture thermal conductivity ranging from 8.96 % to 33.77 %. Additionally, as the limestone sand content increases, the gradation-induced rate of increase in thermal conductivity demonstrates a downward trend, with the most pronounced effect observed in loess-dominated mixtures.

(3) When the moisture content increases from 2 % to 20 %, the influence of gradation on thermal conductivity gradually weakens. However, considering the synergistic effect of moisture content and gradation, the absolute value of the material's thermal conductivity still shows an upward trend. In scenarios where the underground moisture content is relatively high and sandy soil mixtures are employed for backfilling, it is recommended to optimize the gradation. This approach can enhance the thermal conductivity of the backfill material and improve its density, thereby ensuring better performance and stability.

(4) A predictive model for the thermal conductivity of limestone sand-loess mixed materials was developed utilizing a reverse neural network. The $R^2$, MAE, MAPE, and RMSE results for both the training and testing sets demonstrate that the model effectively captures the majority of patterns and information present in the training data, making it applicable to new datasets. The MAPE values achieved were 4.8 % for the training set and 6.4 % for the testing set. Consequently, this model can serve as a valuable tool in guiding the design of thermal conductivity for limestone sand-loess mixtures intended for use as backfill materials.

This article primarily focuses on the preparation of samples through indoor experiments and investigates the effects of dry density, moisture content, and particle gradation on the thermal conductivity of sandy soil mixtures. It underscores the significance of particle gradation on the thermal conductivity of the materials under varying moisture contents and establishes a thermal conductivity prediction model utilizing a reverse neural network. The limitations of the current study are associated with the selection of factors, which solely encompass gradation, dry density, and moisture content. In practical applications, the factors influencing the thermal conductivity of materials are considerably more intricate, and stratified variations in underground rock and soil bodies may also affect the efficiency of material backfilling. Consequently, further research is warranted in future endeavors. Subsequent studies will delve deeper into the application of mixed materials in practical engineering, conduct cost-saving analyses, and further investigate the compressive strength and erosion resistance of mixed materials.

## CRediT authorship contribution statement

**Xiong Liu:** Writing – review & editing, Writing – original draft, Methodology, Investigation, Data curation, Conceptualization. **Ruiyong Mao:** Visualization. **Zujing Zhang:** Supervision. **Hongwei Wu:** Supervision. **Xing Liang:** Supervision. **Jing Chen:** Conceptualization.

## Declaration of Competing Interest

We declare that we have no financial and personal relationships with other people or organizations that can inappropriately influence our work, there is no professional or other personal interest of any nature or kind in any product, service and/or company that could be construed as influencing the position presented in, or the review of, the manuscript entitled 'The thermal conductivity characteristics and prediction models of limestone sand-yellow soil mixtures'.

## Acknowledgments

The author would like to thank the financial support of the National Natural Science Foundation of China (NO.52168013) and the Guizhou Provincial Science and Technology Projects (No. ZK [2022]151 and No. [2019]1102).

## Data availability

Data will be made available on request.

## References

[1] S. Hähnlein, P. Bayer, G. Ferguson, P. Blum, Sustainability and policy for the thermal use of shallow geothermal energy, Energy Policy 59 (2013) 914.
[2] G.M. Idroes, M. Afjal, M. Khan, M. Haseeb, I. Hardi, T.R. Noviandy, R. Idroes, Exploring the role of geothermal energy consumption in achieving carbon neutrality and environmental sustainability, Heliyon 10 (2024) e40709.
[3] M. Tuschl, T. Kurevija, Revitalization modelling of a mature oil field with bottom-type aquifer into geothermal resource—reservoir engineering and techno-economic challenges, Energies 16 (2023).
[4] N. Xu, M. He, M. Xu, H. Chen, A comprehensive investigation on u-tube ground heat exchanger performance considering insulation layer in deep geothermal system, Case Stud. Therm. Eng. 34 (2022).
[5] W. Zhang, J. Wang, F. Zhang, W. Lu, P. Cui, C. Guan, M. Yu, Z. Fang, Heat transfer analysis of u-type deep borehole heat exchangers of geothermal energy, Energy Build. 237 (2021) 110794.
[6] Z. Zhou, J. Zhang, Z. Li, X. Li, H. Yang, Computational model for the thermal conductivity of soil-rock mixture, Int. J. Heat Mass Tran. 230 (2024) 125745.
[7] K.K. Agrawal, R. Misra, G.D. Agrawal, Improving the thermal performance of ground air heat exchanger system using sand-bentonite (in dry and wet condition) as backfilling material, Renew. Energy 146 (2020) 2008.
[8] S. Dong, G. Liu, T. Zhan, Y. Yao, L. Ni, Performance study of cement-based grouts based on testing and thermal conductivity modeling for ground-source heat pumps, Energy Build. 272 (2022) 112351.

[9] L. Mao, Q. Liu, H. Chen, W. Cheng, A novel model of the anisotropic thermal conductivity of composite phase change materials under compression, Int. J. Heat Mass Tran. 227 (2024) 125512.
[10] Z. Zhou, Q. Liu, Y. Tao, Y. Peng, T. Zhou, Y. Wang, Analysis of a borehole ground heat exchanger with shape-stabilized phase change material backfill, Appl. Therm. Eng. 222 (2023) 119925.
[11] D. Pahud, B. Matthey, Comparison of the thermal performance of double u-pipe borehole heat exchangers measured in situ, Energy Build. 33 (2001) 503.
[12] S. Wang, Y. Li, L. Wu, X. He, L. Jian, Q. Chen, Investigation on thermal conductivity property and hydration mechanism of graphene-composite cement for geothermal exploitation, Geothermics 104 (2022) 102477.
[13] R. Borinaga-Trevino, P. Pascual-Munoz, D. Castro-Fresno, E. Blanco-Fernandez, Borehole thermal response and thermal resistance of four different grouting materials measured with a TRT, Appl. Therm. Eng. 53 (2013) 13.
[14] Y. Kim, B.H. Dinh, T.M. Do, G. Kang, Development of thermally enhanced controlled low-strength material incorporating different types of steel-making slag for ground-source heat pump system, Renew. Energy 150 (2020) 116.
[15] J. Zhao, G. Huang, Y. Guo, Z. Feng, R. Gupta, W.V. Liu, Development of a novel cement-based grout with enhanced thermal and sealing performance for borehole heat exchangers, Energy Build. 302 (2024) 113754.
[16] F. Tang, H. Nowamooz, Factors influencing the performance of shallow borehole heat exchanger, Energy Convers. Manag. 181 (2019) 571.
[17] S.W. Carlson, GSHP bore field performance comparisons of standard and thermally enhanced grout, Build. Eng. 106 (2000) 442.
[18] H. Javadi, S. Mousavi Ajarostaghi, M. Rosen, M. Pourfallah, A comprehensive review of backfill materials and their effects on ground heat exchanger performance, Sustainability 10 (2018).
[19] M.D. Smith, R.L. Perry, Borehole grouting: field studies and therm performance testing, Build. Eng. (1999) 105.
[20] S. Wang, Y. Ji, S. He, J. Gao, Y. Wang, X. Cai, Study on heat transfer performance of a ground heat exchanger under different heat transfer mechanisms, Case Stud. Therm. Eng. 51 (2023).
[21] C. Lee, K. Lee, H. Choi, H.P. Choi, Characteristics of thermally-enhanced bentonite grouts for geothermal heat exchanger in South Korea, Sci. China Ser. Tech. Sci. Engl. Edit. New Ser. 53 (2010) 123–128.
[22] F. Tong, L. Jing, R.W. Zimmerman, An effective thermal conductivity model of geological porous media for coupled thermo-hydro-mechanical systems with multiphase flow, Int. J. Rock Mech. Min. Sci. 46 (2009) 1358.
[23] J. Desmedt, J.V. Bael, H. Hoes, N. Robeyn, Experimental performance of borehole heat exchangers and grouting materials for ground source heat pumps, Int. J. Energy Res. 36 (2012) 1238.
[24] D. Kong, R. Wan, The effect of conglomerations gradation on engineering properties of loess, Rev. Constr. 18 (2019) 375.
[25] F. Delaleux, X. Py, R. Olives, A. Dominguez, Enhancement of geothermal borehole heat exchangers performances by improvement of bentonite grouts conductivity, Appl. Therm. Eng. 33 (2012) 92.
[26] D. Kong, R. Wan, J. Chen, J. Kang, X. Jiao, Effect of gradation on the thermal conductivities of backfill materials of ground source heat pump based on loess and iron tailings, Appl. Therm. Eng. 180 (2020) 115814.
[27] Y. Xu, Z. Yao, X. Huang, Y. Fang, S. Shu, H. Zhu, Heat transfer characteristics and heat conductivity prediction model of waste steel slag–clay backfill material, Therm. Sci. Eng. Prog. 46 (2023) 102203.
[28] T. Wen, X. Chen, Y. Luo, L. Shao, G. Niu, Three-dimensional pore structure characteristics of granite residual soil and their relationship with hydraulic properties under different particle gradation by x-ray computed tomography, J. Hydrol. 618 (2023) 129230.
[29] B.H. Nagaraj, Influence of gradation and proportion of sand on stress–strain behavior of clay–sand mixtures, Int. J. Geo Eng. 7 (2016) 1.
[30] L. Wu, J. Li, Y. Huang, P. Huang, C. Yang, Z. Ding, H. Yu, Mesoscopic influence mechanism of particle fragmentation on compressive deformation of gangue aggregates with different gradations under load, Miner. Eng. 217 (2024) 108893.
[31] Z. Ju, T. Ren, C. Hu, Soil thermal conductivity as influenced by aggregation at intermediate water contents, Soil Sci. Soc. Am. J. 75 (2011) 26.
[32] Y. Xiao, H. Liu, B. Nan, J.S. McCartney, Gradation-dependent thermal conductivity of sands, J. Geotech. Geoenviron. Eng. 144 (2018).
[33] J. Bi, Y. Pan, S. Yang, G. Zhao, Z. Wu, A thermal conductivity model for granular geomaterials with low porosity during the freezing process, Int. J. Heat Mass Tran. 233 (2024) 126050.
[34] L. Tang, S. Sun, J. Zheng, P. Qiu, T. Guo, Thermal conductivity changing mechanism of frozen soil-rock mixture and a prediction model, Int. J. Heat Mass Tran. 216 (2023) 124529.
[35] N. Zhang, Z. Wang, Review of soil thermal conductivity and predictive models, Int. J. Therm. Sci. 117 (2017) 172.
[36] A. Alrtimi, M. Rouainia, S. Haigh, Thermal conductivity of a sandy soil, Appl. Therm. Eng. 106 (2016) 551.
[37] Q. Wang, R. Bai, Z. Zhou, W. Zhu, Evaluating thermal conductivity of soil-rock mixtures in Qinghai-Tibet plateau based on theory models and machine learning methods, Int. J. Therm. Sci. 204 (2024) 109210.
[38] X. Li, J. Zhang, W. Ye, X. Liu, X. Sun, A new transient simulation model and changing characteristics for circulating fluid temperature in a deepwater riserless mud recovery system, Ocean Eng. 281 (2023) 114735.
[39] X. Li, J. Zhang, C. Li, W. Chen, J. He, Y. Zheng, R. Li, Characteristic law of borehole deformation induced by the temperature change in the surrounding rock of deep coalbed methane well, J. Energy Resour. Technol. 144 (2021).
[40] X. Li, J. Zhang, X. Tang, C. Li, B. Li, Y. Wang, Z. Zhao, Propagation characteristics and application effects of measurement-while-drilling pressure wave for early gas-kick detection, J. Loss Prev. Process. Ind. 76 (2022) 104741.
[41] K. Li, Q. Kang, J. Nie, X. Huang, Artificial neural network for predicting the thermal conductivity of soils based on a systematic database, Geothermics 103 (2022) 102416.
[42] Y. Wu, Y. Wu, L. Fan, Z. Yu, J.M. Khodadadi, Thermal conductivity of soil: a review on the vast experimental data and predictive models, Int. J. Therm. Sci. 208 (2025) 109486.
[43] A.R. Al-darraji, F. Faraji, Numerical investigation of ribs number effect on heat transfer inside a heated duct, Babylon. J. Mech. Eng. (2024) 26–33.
[44] P. Liu, Z. Han, W. Wu, Y. Zhao, Y. Song, M. Chai, A developed convolutional neural network model for accurately and stably predicting effective thermal conductivity of gradient porous ceramic materials, Int. J. Heat Mass Tran. 225 (2024) 125428.
[45] S. Rehman, S. Algarni, M. Imtiaz, T. Alqahtani, F.A.A. ElSeabee, W. Jamshed, K. Irshad, R.W. Ibrahim, S.M. El Din, Inclined magnetic force impact on cross nanoliquid flowing with widening shallow and heat generating by using artificial neural network (ANN), Case Stud. Therm. Eng. 52 (2023) 103690.
[46] X. Li, J. Zhang, X. Tang, G. Mao, P. Wang, Study on wellbore temperature of riserless mud recovery system by CFD approach and numerical calculation, Petroleum 6 (2020) 163.
[47] J. Zhang, X. Li, X. Tang, et al., Establishment and analysis of temperature field of riserless mud recovery system, Oil Gas Sci. Technol. Rev. d'IFP Energ. Nouv. 74 (2019) 19.
[48] X. Li, J. Zhang, C. Li, B. Li, H. Zhao, R. Li, Q. Qi, Variation characteristics of coal-rock mechanical properties under varying temperature conditions for Shanxi linfen coalbed methane well in China, J. Pet. Explor. Prod. Technol. 11 (2021) 2905.
[49] R. Wan, D. Kong, J. Kang, T. Yin, J. Ning, J. Ma, The experimental study on thermal conductivity of backfill material of ground source heat pump based on iron tailings, Energy Build. 174 (2018) 1.
[50] C.P. Bergmann, Particle size analysis, in: C.P. Bergmann (Ed.), Techniques for Analysis of Mineral Raw Materials, Springer Nature Switzerland, Cham, 2024, p. 87.
[51] Y. Tang, H. Wei, Y. Chen, B. Huang, S. Zhang, Modeling of permeability for granular soils considering the particle size distribution, Granul. Matter 25 (2023) 35.
[52] V. Ravikumar, Soil texture and soil moisture, in: V. Ravikumar (Ed.), Sprinkler and Drip Irrigation: Theory and Practice, Springer Nature Singapore, Singapore, 2023, p. 563.

[53] X. Fu, H. Lyu, Z. Yu, X. Jiang, Y. Ding, D. Zheng, J. Huang, H. Fang, Effects of soil hydraulic properties on soil moisture estimation, J. Meteorol. Res. 37 (2023) 58.
[54] Y. Wang, A. Tran, D.L. McDowell, Chapter one - uncertainty quantification for engineering decision making, in: Y. Wang, A. Tran, D.L. McDowell (Eds.), Fundamentals of Uncertainty Quantification for Engineers, Elsevier, 2025, p. 3.
[55] Ministry of Construction of the People's Republic of China, Technical Code for Ground - Source Heat Pump System (GB 50366 - 2005), China Archit. & Build. Press, 2005.